

# Design and Implementation of DC-to-5 MHz Wide-Bandwidth High-Power High-Fidelity Converter

Jinshui Zhang, *Student Member*, Boshuo Wang, *Member*, Xiaoyang Tian, *Member*, Angel Peterchev, *Member*, and Stefan Goetz, *Member*

**Abstract**—Advances in power electronics have made it possible to achieve high power levels, e.g., reaching GW in grids, or alternatively high output bandwidths, e.g., beyond MHz in communication. Achieving both simultaneously, however, remains challenging. Various applications, ranging from efficient multichannel wireless power transfer to cutting-edge medical and neuroscience applications, are demanding both high power and wide bandwidth. Conventional inverters can achieve high power and high quality at grid or specific frequency ranges but lose their fidelity when reaching higher output frequencies. Resonant circuits can promise a high output frequency but only a narrow bandwidth. We overcome the hardware challenges by combining gallium-nitride (GaN) transistors with modular cascaded double-H bridge circuits and control that can manage typical timing and balancing issues. We developed a lightweight embedded control solution that includes an improved look-up-table digital synthesizer and a novel adaptive-bias-elimination nearest-level modulation. This solution effectively solves the conflict between a high power level and high output bandwidth and can—in contrast to previous approaches—in principle be scaled in both dimensions. Our prototype exhibits a frequency range from DC to 5 MHz with  $< 18\%$  total voltage distortion across the entire frequency spectrum, while achieving a power level of  $> 5$  kW. We conducted tests by sweeping the output frequency and two channel-mixing trials, which included a practical magnetogenetics-oriented stimulation pulse and an entertaining trial to reproduce the famous *Arecibo* message with the current spectrum.

**Index Terms**—Cascaded bridge converter, modular multilevel converter, magnetogenetics, high-frequency modulation, frequency-division multiplexing, wide output bandwidth, nearest level modulation / control

## I. INTRODUCTION

The demands for high-power wide-bandwidth power converters have grown rapidly and widely, driven by applications such as wireless power transfer [1]–[5], power-hardware-in-the-loop systems [6], efficient wide-bandwidth radio-frequency amplifiers [7]–[9], scientific instrumentation [10]–[12], and recent biomedical applications [13]–[20]. Magnetothermogenetics as a cutting-edge neuronal stimulation technique, for instance, uses magnetic fields to remotely control cell activities and particularly inject neuronal signals through activating electromagnetic receivers in the form of nanoparticle–protein compounds [21]. This technology can selectively actuate thermally sensitive ion channel proteins with high-frequency

heating of iron oxide nanoparticles, but requires considerable power and freely tunable high-quality output with low distortion for frequency-multiplexed neural stimulation to avoid activating other nanoparticles with side-bands or harmonics. Additionally, concurrent control of a wider output bandwidth instead of only limited resonances would allow full frequency-division multiplexing for writing neural signals into the brain or for (optionally encrypted) wireless power transfer [22].

Wide output bandwidth from DC to megahertz, high quality, and high efficiency at the same time are challenging conventional power electronics. Typical high-power conversion for electricity grids is best for low frequencies, often as low as the grid frequency, and may offer high power levels but only low bandwidth [23]–[25]. Electric powertrains extend the bandwidth only moderately, typically within the single-digit kilohertz range [26], [26], [27], [27]–[29]. Existing solutions to achieving both higher output frequency and high power mainly involve resonant circuits [19], [30]–[32]. However, the output bandwidth of these circuits is narrow around the resonant frequency. Considerable variation of output frequency requires reconfiguring the hardware [19].

A promising direction for such research is cascaded bridge (CBC) and modular multilevel converters (MMC). These techniques offer a highly scalable and flexible circuit, making them already popular with power delivery and conversion applications, such as high-voltage AC/DC converters [33]–[37] and medium-voltage motor drives [26], [28], [29], [38]–[40]. Furthermore, cascaded circuits spread voltage, current, and switching across a specified number of modules and semiconductors so that they can increase both the output quality and the power–bandwidth product, promising concurrent high bandwidth, high quality, and high power. Previous research has already explored their applications for high-quality pulse synthesizing, demonstrating an output bandwidth in the kHz range and power levels in the MVA range [41]–[44]. However, existing cascaded circuit techniques alone cannot achieve the required DC-to-MHz bandwidth with sufficient power and high quality.

On the one hand, transistors and the circuit topology determine the theoretical output bandwidth of converters. Aiming for a MHz output profile, gallium-nitride (GaN) transistors stand out due to their fast switching dynamics and low parasitic parameters. Balancing of the modules, e.g., with respect to voltage, power, and switching, is another crucial

consideration. The wide bandwidth from DC to MHz rules out most previous options due to their need for module monitoring and sorting, which conflicts with the bandwidth limits of sampling, digital filtering, or sorting algorithms [45]–[50]. The circuit requires a sensorless and fast-responding voltage-sharing method.

On the other hand, the embedded control requires improvement in synthesis and modulation of variable high-bandwidth signals. Traditional synthesis of sinusoidal signals typically relies on look-up tables (LUT) [51]–[54]. However, this method leads to bias when facing high-bandwidth output. Direct digital synthesizer (DDS) technology addresses this issue by introducing a phase accumulator, which requires a tremendous memory size that exponentially increases with the resolution [54]. With limited block memory in embedded controllers, this method degrades into an approach that inherits errors from each output cycle, causing a low-frequency oscillation, i.e., subharmonic distortion [55]. Besides synthesizing, modulating sinusoidal signals also runs into issues at high frequencies. For example, pulse width modulation (PWM) methods, though conventionally popular, struggles with very-high-bandwidth signals due to interactions between the signal and the carrier(s) [56]. Instead, nearest-level modulation (NLM) does not rely on any carrier and offers a wide bandwidth close to the switching rate. However, due to only few clock cycles covering high-frequency output as well as the limited precision number representation in embedded controllers, NLM may suffer from numerical asymmetry errors caused by rounding operations, leading to DC bias or low-frequency oscillations and potentially resulting in over-current.

To address hardware challenges, we combine the cascaded double-H bridge circuit, which supports a fast sensorless voltage balancing method [57]–[61], with GaN transistors to provide both wide output bandwidth and high power level. For the embedded control, we modify the look-up table method to synthesize high-frequency sinusoidal signals in embedded controllers without causing DC bias or oscillation. Additionally, we improve the nearest-level modulation to adaptively eliminate the numeric error due to limited precision.

## II. CONCEPT

### A. Circuit

Figure 1 describes the circuit configuration. The system consists of seven cascaded double-H bridge submodules. The submodules can assume six states, including Bypass+, Bypass-, Series+, Series-, Parallel+ and Parallel-, respectively generating an output of  $\{0, 0, +V, -V, 0, 0\}$  [40], [62]. Parallel connectivity simplifies the overall topology of the high-voltage DC bus, rendering the necessity for just a single low-voltage DC source, which is then connected to the fourth module as depicted in Figure 1 [62]. The system architecture incorporates GaN enhancement-mode transistors due to their capability for MHz-level switching rates.

The standout advantage of this topology is its capability for sensorless voltage balancing. The double-H bridge configuration achieves voltage equilibrium across modules through rapid paralleling, resulting in modestly increased switching

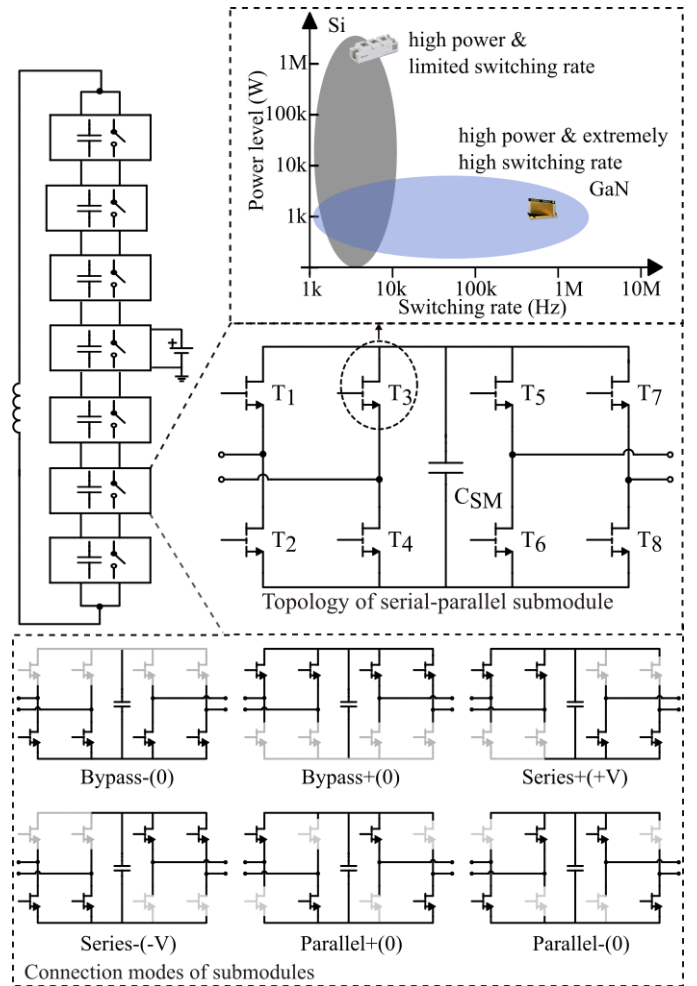


Fig. 1: Single-arm demonstration circuit consisting of seven GaN-based parallel-series modules. Each module has two H-bridges and can generate an output level of zero, positive or negative capacitor voltage. The double H-bridge structure enables parallel connectivity and thus ideally balanced voltage among modules. GaN transistors offer high switching rates, enabling theoretically high output frequencies.

loss, though [63]. This approach ensures efficient energy distribution among modules without necessitating monitoring or sorting procedures, which run into limitations at the required speeds.

On the other hand, it is important to recognize the trade-off between the frequency at which modules clear their imbalance through parallelization, which can drive switching loss, and the energy loss caused by parallelization, if the modules had too much time building up a significant imbalance. A faster paralleling process leads to reduced losses during parallelization, but at the expense of increased switching losses.

### B. Embedded Control Design

1) *Reference Signal Synthesis*: The initial stage of the control process involves synthesizing the reference signal, which consists of sinusoidal signals with a wide range of frequencies. Embedded controllers typically synthesize sinusoidal signals

TABLE I: Quantities Definition

Symbol	Quantities or Operation
$f_o$	Objective frequency
$f_{\text{clock}}$	FPGA clock rate
$k$	Index of FPGA clock within output cycle
$K$	Number of FPGA clocks during each output cycle
$n$	Index of output cycle
$L$	Length of look-up table
$A(k)$	Address of look up table at $k$ -th FPGA clock
$A_0(n)$	Initial address of $n$ -th output cycle of look up table
$\Delta A$	Address increment for each FPGA clock
$s_{\text{ref,fp}}$	Reference signal, fixed-point numbers
$s_{\text{mod,inte}}$	Digitized modulation signal, integers

through a look-up table (LUT). However, when aiming to achieve an output frequency spanning up to 5 MHz, the traditional LUT method falls short of delivering the desired output quality.

Key variables in LUT, including the address increment for each FPGA clock, the number of clock cycles of the controller per output cycle, and the index within an output cycle, respectively follow

$$\begin{aligned} \Delta A &= L \frac{f_o}{f_{\text{clock}}} \\ K &= \left\lfloor \frac{L}{\Delta A} \right\rfloor \\ k &\in \{0, 1, \dots, K-1\}. \end{aligned} \quad (1)$$

A sinusoidal reference waveform of predefined length  $L$  is stored in the embedded controller. Flip-flops can optionally offer faster reading rates or memory for accommodating larger table sizes. If the output frequency  $f_o$  remains constant, we can optimize the length of the look-up table to ensure symmetric table value visits during one output cycle, thereby guaranteeing a zero net accumulation. Nevertheless, when the output frequency varies, the conventional LUT method falls short of covering the complete frequency range without resulting in DC bias in the output voltage and subsequent excessive over-current.

For every output cycle, the conventional LUT method starts visiting the table at  $A_0 = 0$ . However, this method can lead to non-zero summation and thus a DC bias,  $\sum A(k) \neq 0$ . We can handle DC bias error by starting the address from a non-zero initial address for each output cycle per

$$A_0(n) = (A_K(n-1) + \Delta A) - L, \quad (2)$$

where  $A_K(n-1)$  is the last address of the  $(n-1)$ -th output cycle,  $A_0(n)$  the first address of the  $n$ -th output cycle. By inheriting errors of the previous cycle, the lookup table will be repeated circularly, and the accumulated net value alternates with a zero average. This method can effectively reduce the DC bias and prevent the circuit from damage caused by infinite current in the inductor load. However, an issue with this LUT method is that it leads to a periodically alternating net value. Instead of generating a DC bias in the output, there is a low-frequency (LF) oscillation caused by the periodically changing

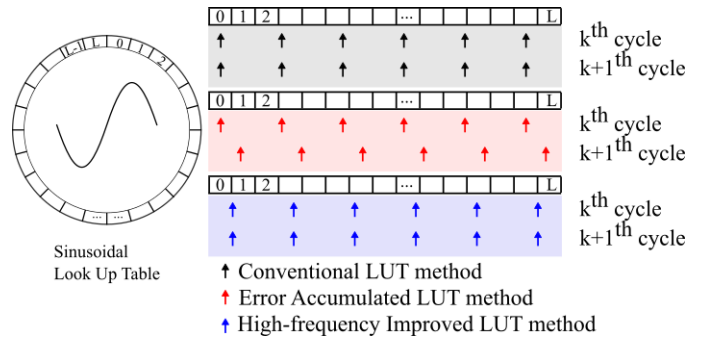


Fig. 2: Principles of different LUT methods, respectively, a) The conventional LUT approach, which always visits from zero for every output cycle; b) The error-inherited LUT approach, which visits the table from the bias address obtained from the last output cycle; c) The improved LUT method, which starts from an initial address that is pre-calculated according to the output frequency and avoids DC bias or low-frequency oscillation.

net value for each individual cycle. The frequency of the oscillation is obtained with

$$f_{\text{LF}} = \frac{\Delta A}{(L - K * \Delta A)} \quad (3)$$

Here we propose an improved LUT method. This LUT method starts with the same initial address for each output cycle. The initial address is derived as follows by ensuring a zero-net value for each individual cycle. This requires the middle point of the lookup table results to be exactly at phase  $\pi$ . For a sinusoidal LUT, suppose  $K$  is odd, then

$$A\left(\frac{K-1}{2}\right) = 0. \quad (4)$$

If  $K$  is even, then

$$A\left(\frac{K}{2}\right) + A\left(\frac{K}{2} + 1\right) = 0, \quad (5)$$

i.e.,

$$A\left(\frac{K+1}{2}\right) = 0. \quad (6)$$

If  $\lfloor f_{\text{clock}}/f_o \rfloor$  is odd, the initial address should satisfy

$$A_0 + \frac{K-1}{2} \Delta A = \frac{L}{2}. \quad (7)$$

If even, it should instead satisfy

$$A_0 + \left(\frac{K}{2} - 1\right) * \Delta A + \frac{1}{2} \Delta A = \frac{L}{2}. \quad (8)$$

Combining both scenarios, we can obtain the universal expression of the initial address:

$$A_0 = \frac{L}{2} - \frac{K-1}{2} \Delta A \quad (9)$$

By applying the proposed LUT method, the reference signal can promise a net-zero value for any output cycle.

The proposed LUT method can theoretically synthesize correct sinusoidal pulses over the full bandwidth. However, the modulation method fails to cover the full frequency and

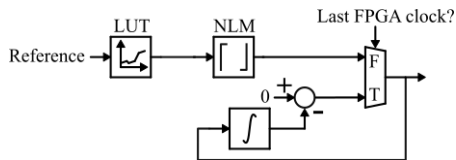


Fig. 3: Diagram of the bias-eliminating nearest level modulation approach. This modified NLM method integrates the rounding integers periodically, and feeds the result back to the output of NLM at the end of each output cycle, maintaining a same behavior as the conventional approach at low frequencies but avoiding distortion at high frequencies.

amplitude range without causing output errors. Nearest-level modulation works by rounding the continuous reference signal to the nearest integer levels represented by multilevel output voltage steps, requiring only fundamental frequency switching:

$$s_{o,inte} = \lfloor s_{in} \rfloor \quad (10)$$

High-frequency reference signals allow only a limited number of modulation clock ticks within one output cycle. Since the advanced LUT method generate a reference signal that centers at the phase  $\pi$ , the reference signal is symmetric around  $(\pi, 0)$ . Theoretically, the digitized signal after NLM would still be symmetric and lead to a zero-sum for each individual output cycle. However, performing with modulation amplitude and limited length of representation for fixed-point variables in embedded controller can cause cases where the digitization still exposes a DC bias. Increasing the length of registers could reduce but will not eliminate the possibility of such implementation abnormality:

$$\begin{aligned} \sum s_{ref,fp} &= 0 \\ \sum s_{mod,inte} &\neq 0 \end{aligned} \quad (11)$$

We propose a modified NLM method that can adaptively eliminate the numerical error for high-frequency sinusoidal modulation. This modulation strategy ensures a zero accumulation value for each output cycle:

$$s_{mod,K} = 0 - \sum_{k=1}^{K-1} s_{mod,k} \quad (12)$$

As per (12) and Fig. 3, the accumulation value is compared with zero at the end of the output cycle. The difference decides the last output command. Thus, the modulation can adaptively modify the output commands to achieve a net-zero value for each individual output cycle.

In summary, the embedded control solves two crucial problems, respectively the synthetization of high-frequency sinusoidal signals with an improved LUT method, and their modulation with a modified NLM approach that can adaptively eliminate distortion.

### III. SIMULATION VERIFICATION OF EMBEDDED CONTROL METHOD

The software aims for seamless operation across the entire bandwidth, spanning from DC to 5 MHz, while maintaining

TABLE II: Key components in prototype design

Item	Product Information
Transistor	GS61008T (100V, 7 mΩ, GaN Systems)
Transistor driver IC	ACPL-P346-000E (2.5 A, BroadCom)
Power supply	HP 6030A (200V/17A, 1200 W, Agilent)
Embedded controller	sbRIO-9627 (Zynq-7020 FPGA, National Instruments)

TABLE III: Measurement tools

Item	Product Information
Oscilloscope	MDO3054 (500 MHz, 2.5 GSPS, Tektronix)
Voltage probe	THDP0100 (100 MHz, 2.3 kV, Tektronix)
Current probe	HF60R (30 MHz, CWTMini, PEM)
Spectrogram program	matplotlib.pyplot.specgram (Python Package)

amplitude range integrity, without introducing a DC bias or significant distortion.

In our simulation, modulation factors ranged from 0 to 1 in increments of 0.01, and frequencies from 1 kHz to 5 MHz in 1 kHz steps. Four distinct software approaches were evaluated: zero-started LUT with NLM, error-inherited LUT with NLM, improved LUT with NLM, and improved LUT with adaptively-error-eliminating NLM.

The output current behavior can be categorized into three groups: the ideal case, DC bias, and low-frequency oscillation. DC bias and low-frequency oscillation both result in over-current situations, with the former leading to excessive current and the latter interfering with other frequency channels.

Figure 4 compares these software implementations. The conventional LUT method displays prominent DC bias, particularly at higher frequencies. The error-inherited LUT method is susceptible to low-frequency oscillation, especially at elevated frequencies. The improved LUT method significantly mitigates DC bias and low-frequency oscillation, though due to embedded controller limitations, a DC bias risk remains. Conversely, the adaptively-error-eliminating NLM method ensures optimal output results across the entire frequency and amplitude range, satisfying the prototype's performance criteria.

Figure 5 provides a statistical overview of modulation outcomes. Existing LUT methods exhibit distortion across a broad frequency range. The proposed LUT method effectively addresses most issues, except for minor defects at lower frequencies. Incorporating the bias-eliminating NLM approach successfully resolves modulation challenges.

## IV. EXPERIMENTAL RESULTS

### A. Setup

In this section, we present the high-power and wide-bandwidth capability with frequency sweeping, i.e., a chirp signal, and showcase the prototype with variously featured output profiles.

We designed and constructed the prototype as illustrated in Figure 6 with key parameters as per Table II and tools from Table III to demonstrate the key improvements over the state of the art, specifically achieving high quality of the current output (indicated by the distortion), e.g., needed to drive magnetic fields, and wide-bandwidth output through switching power electronics with its high power and efficiency capabilities.

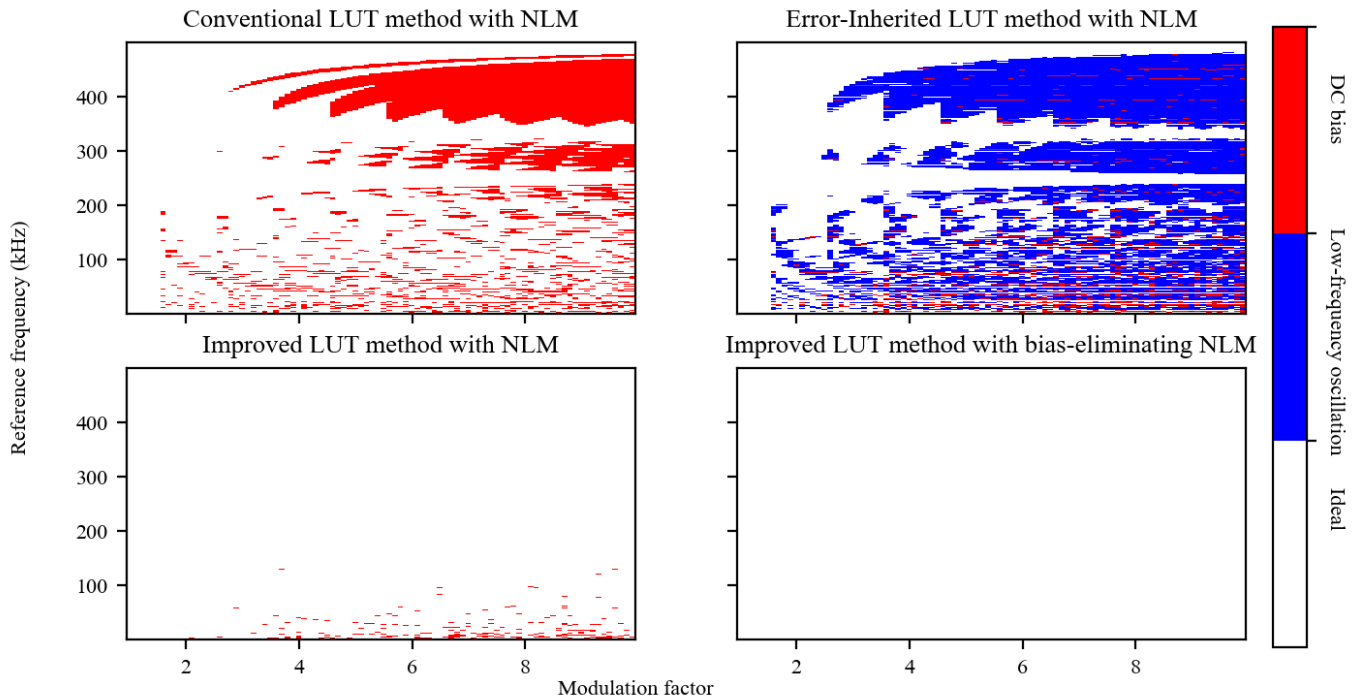


Fig. 4: Comparative analysis of four different LUT methods and modulation configurations: conventional LUT, error-inherited LUT, improved LUT with original NLM method, and improved LUT with adaptively-bias-eliminating NLM. The simulation encompasses a wide frequency range up to 5 MHz and an amplitude range to full modulation. Three output scenarios are observable: ideal performance, DC bias issue, and low-frequency oscillation issue. Conventional and error-inherited LUT methods exhibit notable DC bias or low-frequency distortion. The improved LUT method largely mitigates these issues, occasionally revealing minor imperfections. These rare imperfections are effectively addressed by the bias-eliminating NLM approach.

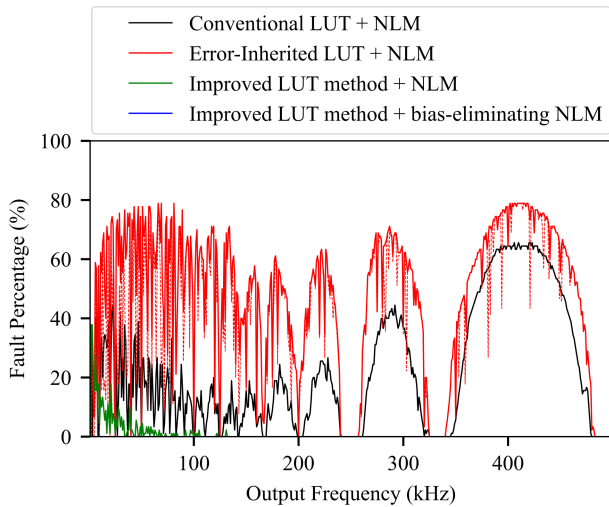


Fig. 5: Quantitative perspective of modulation simulation results over output frequency, i.e., a quantitative presentation of results in Fig. 4, which intuitively compares the distribution of modulation performance over frequency and amplitude.

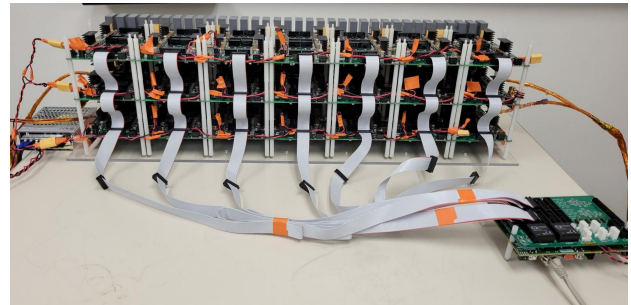


Fig. 6: High-power wide-bandwidth prototype hardware of the circuit.

### B. Sweeping-Frequency Output: Characterizing Power and Bandwidth Capability as well as Fidelity

Figure 7 demonstrates the spectrogram of a frequency sweep from DC to 5 MHz in 1 ms, while maintaining a widely constant voltage amplitude at full modulation factor. The peak voltage level of 140 V corresponds to the sum of the module voltages ( $7 \times 20$  V). Due to the inductive load, the current is decreasing from initially some 50 A with rising frequency.

The total voltage distortion remains consistently below 18.4%, with an average distortion of 17.74% across the frequency spectrum. Due to switching, most distortion is in

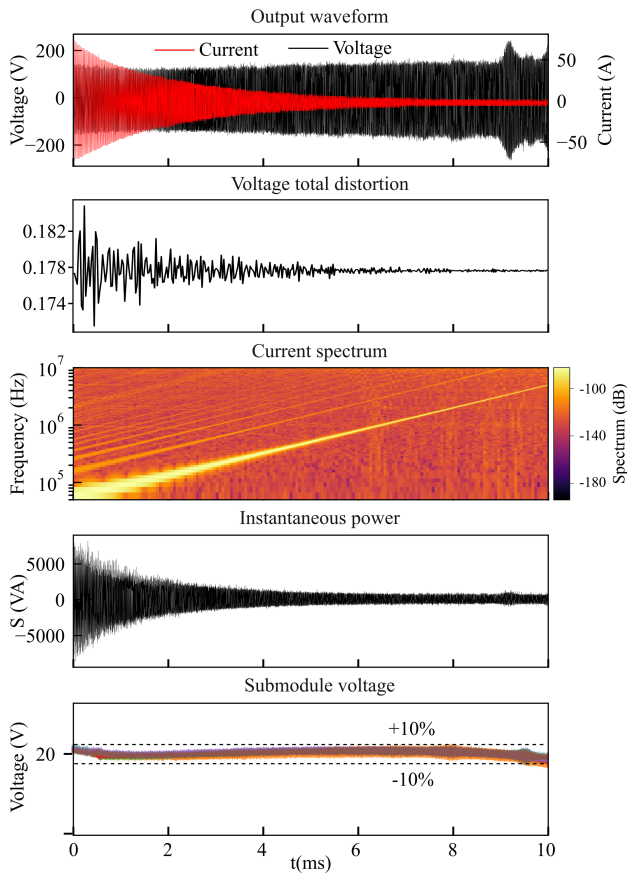


Fig. 7: Frequency sweeping demonstrated with a chirp signal that exponentially increases frequency from DC to 5 MHz within 10 ms.

regular harmonics as the parallel lines in the current spectrogram demonstrate. The balancing solution keeps the voltages of the submodules within a range of  $\pm 2$  V (equivalent to  $\pm 10\%$ ).

### C. Frequency Mixing

TABLE IV: Summary of Channel Mixture Presentation

Frequency	Normalized voltage amplitude	Interval
100 kHz	2	0 ~ 200 $\mu$ s
200 kHz	4	100 ~ 500 $\mu$ s
400 kHz	3	400 ~ 800 $\mu$ s
1 MHz	4	600 ~ 700 $\mu$ s
3 MHz	4	700 ~ 800 $\mu$ s
5 MHz	6	800 ~ 1000 $\mu$ s

Various applications, such as multichannel wireless power transfer, inductive power encryption, and magnetogenetics for various frequency-selective nanoparticles require the independent generation and control of several frequencies, including independent amplitude variation and frequency modulation. Figure 8 demonstrates such frequency-division signals in voltage, current, and spectrogram with the components listed in Table IV. The fundamental mode at 10 kHz is maintained, while higher-frequency channels are mixed in.

The spectra of each interval of Fig. 8 lead to sharp lines in Fig. 9, only broadened by the window lengths.

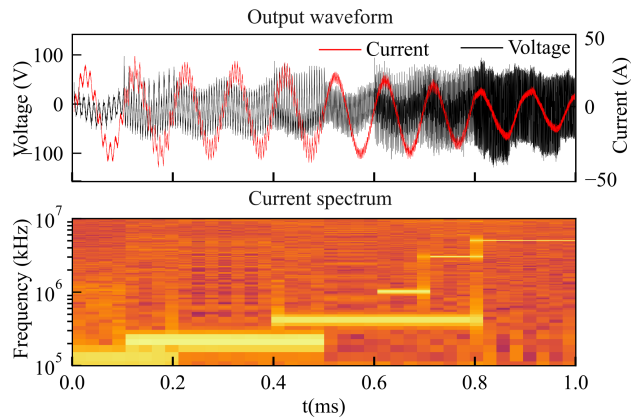


Fig. 8: Neuronal stimulation oriented channels-mixture trial. 7 channels are selected to activate potential magnetic nanoparticles. Each channel is activated with specified amplitude and interval.

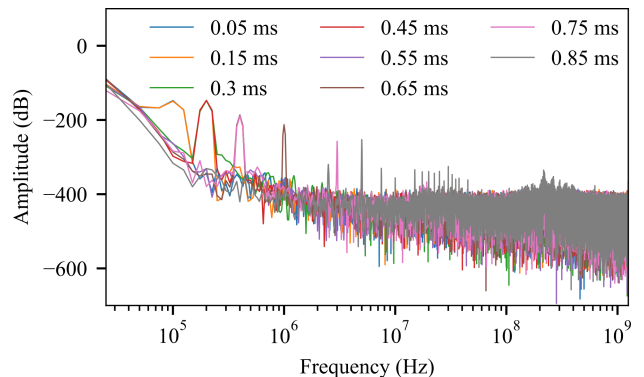


Fig. 9: Fourier transformation analysis of the experiment in Fig. 8 at moments that cover all diverse combinations of frequency channels.

### D. Arbitrary Multifrequency Output

The circuit with the control can modulate the signal fast enough to serve as a signal amplifier. Figure 10 displays the measurement of the Arecibo message sent through our magnetic antenna [64].

Furthermore, this technique holds promise for encrypted communication. By employing customized sequences of frequency channels instead of linearly natural ones, the received information or image would resemble a confounding puzzle, akin to having undergone a paper shredder. Only when the correct frequencies and sequence are supplied does the received information coalesce into a coherent form.

## V. CONCLUSION

This paper demonstrated the generation of concurrent high power and high bandwidth with high quality with a combination of several measures. The power-bandwidth product exceeded  $25 \text{ GV} \cdot \text{A} \cdot \text{Hz}$ , which exceeds the state of the art, whose figures lie  $10 \sim 100 \text{ MV} \cdot \text{A} \cdot \text{Hz}$ , by more than 2 orders of magnitude, and a total distortion (or THD+N) of 17%. In contrast to monolithic circuits, the cascaded design allows further scaling for even higher levels.

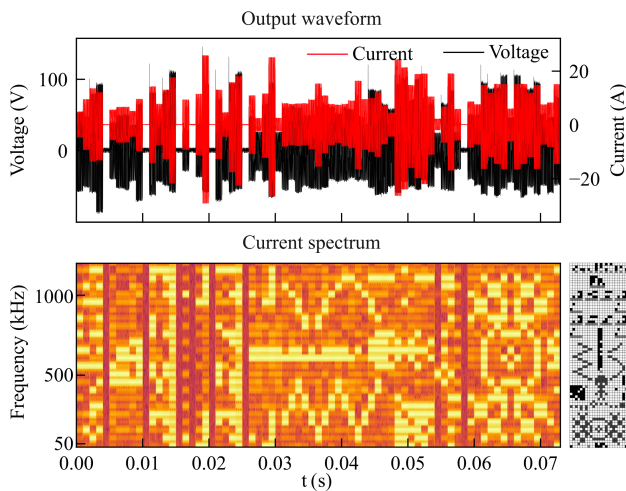


Fig. 10: Arecibo reply message is compressed in the current spectrogram. 23 frequency channels, respectively 50 kHz, 100 kHz, linearly increasing to 1150 kHz with 50 kHz step size, are used to reproduce the message within 73 ms, representing 23 x 73 pixels in the original message.

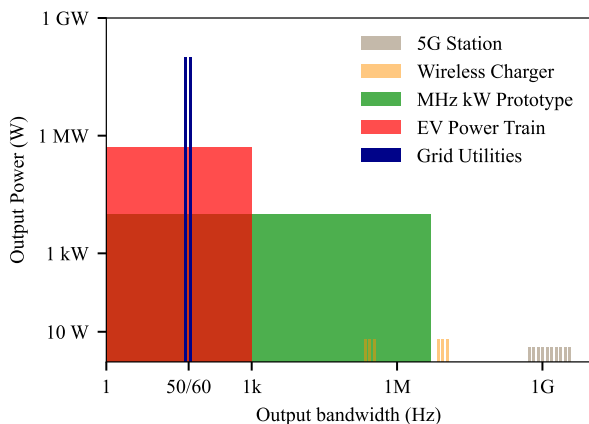


Fig. 11: Prototype capability demonstration compared with other power converters.

As no single ingredient alone was able to achieve the target values, we combined a cascaded bridge circuit, fast-switching GaN transistors, and proper embedded control. Modules allowing dynamic series and parallel inter-module connectivity enabled stable and fast sensor-less module balancing.

We demonstrated the prototype's abilities to generate rapidly changing wide-bandwidth signals in the kilowatt range.

The solution overcomes the previous limitation of concurrent power, bandwidth, and quality. Whereas conventional monolithic circuits, both resonant and hard-switching, have a fixed product of these values, the cascaded topology allows scaling all three of them by adding additional modules that share power, improve the quantization granularity, and spread the necessary switching speed out.

Various applications from multi-channel inductive power transfer, wireless energy encryption, combined power and signal transmission to medical implants, and magnetogenetics

may immediately benefit from the development.

## ACKNOWLEDGMENT

This research was developed with funding from the Defense Advanced Research Projects Agency (DARPA) of the United States of America, Contract No. N66001-19-C-4020. The presented views, opinions and/or findings are those of the authors and should not be interpreted as representing the official views or policies of the Department of Defense or the U.S.A. Government.

## REFERENCES

- [1] C. Qi, S. Huang, X. Chen, and P. Wang, "Individual output voltage regulation method of multifrequency multireceiver simultaneous wpt systems with a single inverter," *IEEE Journal of Emerging and Selected Topics in Power Electronics*, vol. 11, DOI 10.1109/JESTPE.2022.3212447, no. 1, pp. 1245–1261, 2023.
- [2] X. Tian, K. T. Chau, H. Pang, and W. Liu, "Power adaption design for multifrequency wireless power transfer system," *IEEE Transactions on Magnetics*, vol. 58, DOI 10.1109/TMAG.2021.3132959, no. 8, pp. 1–5, 2022.
- [3] W. Jin, A. T. L. Lee, S.-C. Tan, and S. Y. Hui, "A gallium nitride (gan)-based single-inductor multiple-output (simo) inverter with multi-frequency ac outputs," *IEEE Transactions on Power Electronics*, vol. 34, DOI 10.1109/TPEL.2019.2896649, no. 11, pp. 10 856–10 873, 2019.
- [4] S. Liu, Y. Wu, L. Zhou, R. Mai, Z. He, and S. M. Goetz, "A two-dimensional misalignment-tolerant ipt system based on three-arm voltage doubler rectifier," in *2022 IEEE Energy Conversion Congress and Exposition (ECCE)*, DOI 10.1109/ECCE50734.2022.9947537, pp. 1–7, 2022.
- [5] X. Tian, K. T. Chau, W. Liu, and C. H. T. Lee, "Selective wireless power transfer using magnetic field editing," *IEEE Transactions on Power Electronics*, vol. 36, DOI 10.1109/TPEL.2020.3017000, no. 3, pp. 2710–2719, 2021.
- [6] J. BÄhler, J. Huber, J. Wurz, M. Stransky, N. Uvaidov, S. Srdic, and J. W. Kolar, "Ultra-high-bandwidth power amplifiers: A technology overview and future prospects," *IEEE Access*, vol. 10, DOI 10.1109/ACCESS.2022.3172291, pp. 54 613–54 633, 2022.
- [7] A. Sepahvand, P. Momenroodaki, Y. Zhang, Z. Popovic, and D. Maksimovic, "Monolithic multilevel gan converter for envelope tracking in rf power amplifiers," in *IEEE Energy Conversion Congress and Exposition (ECCE)*, DOI 10.1109/ECCE.2016.7855275, pp. 1–7, 2016.
- [8] M. Vasic, O. Garcia, J. A. Oliver, P. Alou, D. Diaz, and J. A. Cobos, "Multilevel power supply for high-efficiency rf amplifiers," *IEEE Transactions on Power Electronics*, vol. 25, DOI 10.1109/TPEL.2009.2033186, no. 4, pp. 1078–1089, 2010.
- [9] M. Rodriguez, P. Miaja, A. Rodriguez, and J. Sebastian, "Multi-level converter for envelope tracking in rf power amplifiers," in *IEEE Energy Conversion Congress and Exposition, ECCE*, DOI 10.1109/ECCE.2009.5316317, pp. 503–510, 2009.
- [10] J. Ma, L. Yu, S. Dong, C. Yao, L. Gao, W. Sun, and Y. He, "Mhz nanosecond rectangular pulse generator with high voltage gain and multimode," *IEEE Transactions on Power Electronics*, vol. 36, DOI 10.1109/TPEL.2021.3052943, no. 8, pp. 8978–8987, 2021.
- [11] J. W. Simonaitis, B. Slayton, Y. Yang-Keathley, P. D. Keathley, and K. K. Berggren, "Precise, subnanosecond, and high-voltage switching enabled by gallium nitride electronics integrated into complex loads," *Review of Scientific Instruments*, vol. 92, DOI 10.1063/5.0046706, no. 7, p. 074704, 2021. [Online]. Available: doi.org/10.1063/5.0046706
- [12] R. Visintini, K. Cautero, C. Martins, G. Goransson, and M. Collins, "Power converters for the magnets of the linac warm units of ess," in *Annual Conference of the IEEE Industrial Electronics Society, IECON*, vol. 42, DOI 10.1109/IECON.2016.7794102, pp. 3552–3557, 2016.
- [13] K. Hayashi, K. Ono, H. Suzuki, M. Sawada, M. Moriya, W. Sakamoto, and T. Yogo, "High-frequency, magnetic-field-responsive drug release from magnetic nanoparticle/organic hybrid based on hyperthermic effect," *ACS applied materials & interfaces*, vol. 2, no. 7, pp. 1903–1911, 2010.
- [14] A. Monsalve, A. C. Bohórquez, C. Rinaldi, and J. Dobson, "Remotely triggered activation of tgf-with magnetic nanoparticles," *IEEE Magnetics Letters*, vol. 6, pp. 1–4, 2015.

- [15] H. Oliveira, E. Pérez-Andrés, J. Thevenot, O. Sandre, E. Berra, and S. Lecommandoux, "Magnetic field triggered drug release from polymersomes for cancer therapeutics," *Journal of Controlled Release*, vol. 169, no. 3, pp. 165–170, 2013.
- [16] H. Huang, S. Delikanli, H. Zeng, D. M. Ferkey, and A. Pralle, "Remote control of ion channels and neurons through magnetic-field heating of nanoparticles," *Nature nanotechnology*, vol. 5, no. 8, pp. 602–606, 2010.
- [17] R. Chen, G. Romero, M. G. Christiansen, A. Mohr, and P. Anikeeva, "Wireless magnetothermal deep brain stimulation," *Science*, vol. 347, no. 6229, pp. 1477–1480, 2015.
- [18] R. Munshi, S. M. Qadri, Q. Zhang, I. C. Rubio, P. Del Pino, and A. Pralle, "Magnetothermal genetic deep brain stimulation of motor behaviors in awake, freely moving mice," *Elife*, vol. 6, p. e27069, 2017.
- [19] B. Wang, Z. Li, C. Sebesta, D. T. Hinojosa, Q. Zhang, J. T. Robinson, G. Bao, A. V. Peterchev, and S. M. Goetz, "Multichannel power electronics and magnetic nanoparticles for selective thermal magnetogenetics," *Journal of Neural Engineering*, vol. 19, DOI 10.1088/1741-2552/ac5b94, no. 2, p. 026015, Mar. 2022. [Online]. Available: <https://doi.org/10.1088/1741-2552/ac5b94>
- [20] S. M. Goetz and Z.-D. Deng, "The development and modelling of devices and paradigms for transcranial magnetic stimulation," *International Review of Psychiatry*, vol. 29, no. 2, pp. 115–145, 2017.
- [21] C. Sebesta, D. Torres Hinojosa, B. Wang, J. Asfour, Z. Li, G. Duret, K. Jiang, Z. Xiao, L. Zhang, Q. Zhang *et al.*, "Subsecond multichannel magnetic control of select neural circuits in freely moving flies," *Nature Materials*, vol. 21, no. 8, pp. 951–958, 2022.
- [22] Z. Zhang, K. T. Chau, C. Qiu, and C. Liu, "Energy encryption for wireless power transfer," *IEEE Transactions on Power Electronics*, vol. 30, DOI 10.1109/TPEL.2014.2363686, no. 9, pp. 5237–5246, 2015.
- [23] H. Abu Bakar Siddique, A. R. Lakshminarasimhan, C. I. Odeh, and R. W. De Doncker, "Comparison of modular multilevel and neutral-point-clamped converters for medium-voltage grid-connected applications," in *2016 IEEE International Conference on Renewable Energy Research and Applications (ICRERA)*, DOI 10.1109/ICRERA.2016.7884555, pp. 297–304, 2016.
- [24] N. S. Patil and A. Shukla, "Review and comparison of mv grid-connected extreme fast charging converters for electric vehicles," in *2021 National Power Electronics Conference (NPEC)*, DOI 10.1109/NPEC52100.2021.9672538, pp. 1–6, 2021.
- [25] S. Rivera, S. M. Goetz, S. Kouro, P. W. Lehn, M. Pathmanathan, P. Bauer, and R. A. Mastromauro, "Charging infrastructure and grid integration for electromobility," *Proc. IEEE*, vol. 111, DOI 10.1109/JPROC.2022.3216362, no. 4, pp. 371–396, 2023.
- [26] M. Spichartz, V. Staudt, and A. Steimel, "Analysis of the module-voltage fluctuations of the modular multilevel converter at variable speed drive applications," in *2012 13th International Conference on Optimization of Electrical and Electronic Equipment (OPTIM)*, DOI 10.1109/OPTIM.2012.6231806, pp. 751–758, 2012.
- [27] B. Li, J. Hu, S. Zhou, and D. Xu, "Hybrid back-to-back mmc system for variable speed ac machine drives," *CPSS Transactions on Power Electronics and Applications*, vol. 5, DOI 10.24295/CPSS/TPEA.2020.00010, no. 2, pp. 114–125, 2020.
- [28] M. Hagiwara, I. Hasegawa, and H. Akagi, "Startup and low-speed operation of an adjustable-speed motor driven by a modular multilevel cascade inverter (mmci)," in *2012 IEEE Energy Conversion Congress and Exposition (ECCE)*, DOI 10.1109/ECCE.2012.6342749, pp. 718–725, 2012.
- [29] J. E. Huber and A. J. Korn, "Optimized pulse pattern modulation for modular multilevel converter high-speed drive," in *2012 15th International Power Electronics and Motion Control Conference (EPE/PEMC)*, DOI 10.1109/EPEPEMC.2012.6397383, pp. LS1a-1.4-1-LS1a-1.4-7, 2012.
- [30] C. Sebesta, D. Torres, B. Wang, J. Asfour, Z. Li, G. Duret, K. Jiang, Z. Xiao, L. Zhang, Q. Zhang *et al.*, "Sub-second multi-channel magnetic control of select neural circuits in behaving flies," *bioRxiv*, 2021.
- [31] S. A. Q. Mohammed and J.-W. Jung, "A comprehensive state-of-the-art review of wired/wireless charging technologies for battery electric vehicles: Classification/common topologies/future research issues," *IEEE Access*, vol. 9, DOI 10.1109/ACCESS.2021.3055027, pp. 19 572–19 585, 2021.
- [32] A. V. Peterchev, Z.-D. Deng, and S. M. Goetz, "Advances in transcranial magnetic stimulation technology," *Brain stimulation: Methodologies and interventions*, pp. 165–189, 2015.
- [33] S. Allebrod, R. Hamerski, and R. Marquardt, "New transformerless, scalable modular multilevel converters for hvdc-transmission," in *2008 IEEE Power Electronics Specialists Conference*, DOI 10.1109/PESC.2008.4591920, pp. 174–179, 2008.
- [34] R. Marquardt, "Modular multilevel converter: A universal concept for hvdc-networks and extended dc-bus-applications," in *The 2010 International Power Electronics Conference - ECCE ASIA -*, DOI 10.1109/IPEC.2010.5544594, pp. 502–507, 2010.
- [35] K. Friedrich, "Modern hvdc plus application of vsc in modular multilevel converter topology," in *2010 IEEE International Symposium on Industrial Electronics*, DOI 10.1109/ISIE.2010.5637505, pp. 3807–3810, 2010.
- [36] M. Saeedifard and R. Iravani, "Dynamic performance of a modular multilevel back-to-back hvdc system," in *2011 IEEE Power and Energy Society General Meeting*, DOI 10.1109/PES.2011.6038879, pp. 1–1, 2011.
- [37] B. Chuco and E. Watanabe, "Back-to-back hvdc based on modular multilevel converter," in *XI Brazilian Power Electronics Conference*, DOI 10.1109/COBEP.2011.6085335, pp. 970–976, 2011.
- [38] H. Akagi, "New trends in medium-voltage power converters and motor drives," in *2011 IEEE International Symposium on Industrial Electronics*, DOI 10.1109/ISIE.2011.5984128, pp. 5–14, 2011.
- [39] M. Hiller, D. Krug, R. Sommer, and S. Rohner, "A new highly modular medium voltage converter topology for industrial drive applications," in *2009 13th European Conference on Power Electronics and Applications*, pp. 1–10, 2009.
- [40] Z. Li, R. Lizana F., Z. Yu, S. Sha, A. V. Peterchev, and S. M. Goetz, "A modular multilevel series/parallel converter for a wide frequency range operation," *IEEE Transactions on Power Electronics*, vol. 34, DOI 10.1109/TPEL.2019.2891052, no. 10, pp. 9854–9865, 2019.
- [41] Z. Zeng, L. M. Koponen, R. Hamdan, Z. Li, S. M. Goetz, and A. V. Peterchev, "Modular multilevel tms device with wide output range and ultrabrief pulse capability for sound reduction," *Journal of neural engineering*, vol. 19, no. 2, p. 026608, 2022.
- [42] Z. Li, J. Zhang, A. Peterchev, and S. Goetz, "Modular pulse synthesizer for transcranial magnetic stimulation with fully adjustable pulse shape and sequence," *Journal of Neural Engineering*, vol. 19, no. 6, p. 066610, 2022.
- [43] B. Wang, J. Zhang, Z. Li, W. M. Grill, A. V. Peterchev, and S. M. Goetz, "Optimized monophasic pulses with equivalent electric field for rapid-rate transcranial magnetic stimulation," *bioRxiv*, pp. 2022–08, 2022.
- [44] S. M. Goetz, M. Pfaffel, J. Huber, M. Singer, R. Marquardt, and T. Weyh, "Circuit topology and control principle for a first magnetic stimulator with fully controllable waveform," *Proc IEEE Eng Biol Med Conf EMBC*, vol. 34, DOI 10.1109/EMBC.2012.6347016, pp. 4700–4703, 2012. [Online]. Available: [doi.org/10.1109/EMBC.2012.6347016](https://doi.org/10.1109/EMBC.2012.6347016)
- [45] Z. Liu, Z.-x. Liu, C. Li, and C. Fu, "Improved voltage balancing method based on mmc nearest level modulation," in *2017 36th Chinese Control Conference (CCC)*, DOI 10.23919/ChiCC.2017.8029004, pp. 10 359–10 364, 2017.
- [46] H. Miao, J. Mei, J. Zheng, T. Ma, and C. Zhang, "A new mmc control strategy based on one-cycle-control and capacitor voltage balance," in *2015 IEEE 2nd International Future Energy Electronics Conference (IFEEC)*, DOI 10.1109/IFEEC.2015.7361408, pp. 1–5, 2015.
- [47] T. Bandaru, D. Samajdar, P. B. S. Varma, T. Bhattacharya, and D. Chatterjee, "Optimum injection of second harmonic circulating currents for balancing capacitor voltages in hybrid mmc during reduced dc voltage conditions," *IEEE Transactions on Industry Applications*, vol. 56, DOI 10.1109/TIA.2020.2967277, no. 2, pp. 1649–1660, 2020.
- [48] Y. Liu and F. Z. Peng, "A four-level modular multilevel converter with self voltage balancing and extremely small dc capacitor," in *2019 IEEE Applied Power Electronics Conference and Exposition (APEC)*, DOI 10.1109/APEC.2019.8722162, pp. 2865–2871, 2019.
- [49] P. M. Meshram and V. B. Borghate, "A novel voltage balancing method of modular multilevel converter (mmc)," in *2011 International Conference on Energy, Automation and Signal*, DOI 10.1109/ICEAS.2011.6147159, pp. 1–5, 2011.
- [50] K. Wang, L. Zhou, Y. Deng, Y. Lu, C. Wang, and F. Xu, "Application range analysis and implementation of the logic-processed cpswm scheme based mmc capacitor voltage balancing strategy," *CPSS Transactions on Power Electronics and Applications*, vol. 4, DOI 10.24295/CPSS/TPEA.2019.00001, no. 1, pp. 1–9, 2019.
- [51] M. Rusdi, F. A. Samman, and R. S. Sadjad, "Fpga-based electronic pulse generator for single-phase dc/ac inverter," in *2019 International Conference on Information and Communications Technology (ICOIACT)*, DOI 10.1109/ICOIACT46704.2019.8938571, pp. 756–760, 2019.
- [52] J. Long, M. Yang, Y. Chen, Q. Ni, and D. Xu, "Comparative study of voltage source inverter nonlinearity compensation using different signal information for table look up in pmsm drives," in *The 10th International Conference on Power Electronics, Machines and Drives (PEMD 2020)*, vol. 2020, DOI 10.1049/icp.2021.1190, pp. 367–371, 2020.



- [53] T. Abeyasekera, C. Johnson, D. Atkinson, and M. Armstrong, "Elimination of subharmonics in direct look-up table (dlt) sine wave reference generators for low-cost microprocessor-controlled inverters," *IEEE Transactions on Power Electronics*, vol. 18, DOI 10.1109/TPEL.2003.818830, no. 6, pp. 1315–1321, 2003.
- [54] I. Analog Devices. A technical tutorial on digital signal synthesis. (1999). [Online]. Available: <https://www.analog.com/en/education/education-library/technical-tutorial-dds.html>
- [55] T. Kacetl, J. Kacetl, N. Tashakor, J. Fang, and S. M. Goetz, "Bandwidth-increased ripple-mitigating scheduling algorithm for dynamically reconfigurable batteries," *IEEE Access*, vol. 10, DOI 10.1109/ACCESS.2022.3204058, pp. 104 202–104 214, 2022.
- [56] D. G. Holmes and T. A. Lipo, *Pulse width modulation for power converters: principles and practice*, vol. 18. John Wiley & Sons, 2003.
- [57] S. M. Goetz, Z. Li, A. V. Peterchev, X. Liang, C. Zhang, and S. M. Lukic, "Sensorless scheduling of the modular multilevel series-parallel converter: enabling a flexible, efficient, modular battery," in *2016 IEEE Applied Power Electronics Conference and Exposition (APEC)*, DOI 10.1109/APEC.2016.7468193, pp. 2349–2354, 2016.
- [58] J. Fang, Z. Li, and S. M. Goetz, "Multilevel converters with symmetrical half-bridge submodules and sensorless voltage balance," *IEEE Transactions on Power Electronics*, vol. 36, DOI 10.1109/TPEL.2020.3000469, no. 1, pp. 447–458, 2021.
- [59] Z. Li, R. Lizana, A. V. Peterchev, and S. M. Goetz, "Distributed balancing control for modular multilevel series/parallel converter with capability of sensorless operation," in *2017 IEEE Energy Conversion Congress and Exposition (ECCE)*, DOI 10.1109/ECCE.2017.8096011, pp. 1787–1793, 2017.
- [60] Z. Li, R. Lizana, S. Sha, Z. Yu, A. V. Peterchev, and S. M. Goetz, "Module implementation and modulation strategy for sensorless balancing in modular multilevel converters," *IEEE Transactions on Power Electronics*, vol. 34, no. 9, pp. 8405–8416, 2018.
- [61] Z. Li, J. K. Motwani, Z. Zeng, S. M. Lukic, A. V. Peterchev, and S. M. Goetz, "A reduced series/parallel module for cascade multilevel static compensators supporting sensorless balancing," *IEEE Transactions on Industrial Electronics*, vol. 68, no. 1, pp. 15–24, 2020.
- [62] J. Fang, F. Blaabjerg, S. Liu, and S. M. Goetz, "A review of multilevel converters with parallel connectivity," *IEEE Transactions on Power Electronics*, vol. 36, DOI 10.1109/TPEL.2021.3075211, no. 11, pp. 12 468–12 489, 2021.
- [63] S. M. Goetz, A. V. Peterchev, and T. Weyh, "Modular multilevel converter with series and parallel module connectivity: Topology and control," *IEEE Transactions on Power Electronics*, vol. 30, DOI 10.1109/TPEL.2014.2310225, no. 1, pp. 203–215, 2015.
- [64] The Staff at the National Astronomy and Ionosphere Center, "The arecibo message of november, 1974," *Icarus*, vol. 26, DOI [https://doi.org/10.1016/0019-1035\(75\)90116-5](https://doi.org/10.1016/0019-1035(75)90116-5), no. 4, pp. 462–466, 1975. [Online]. Available: <https://www.sciencedirect.com/science/article/pii/0019103575901165>